

An atom interferometer testing the universality of free fall and gravitational redshift

Christian Ufrecht,¹ Fabio Di Pumpo,¹ Alexander Friedrich,¹ Albert Roura,² Christian Schubert,³ Dennis Schlippert,³ Ernst M. Rasel,³ Wolfgang P. Schleich,^{1,2,4} and Enno Giese¹

¹*Institut für Quantenphysik and Center for Integrated Quantum Science and Technology (IQST), Universität Ulm, Albert-Einstein-Allee 11, D-89069 Ulm, Germany*

²*Institute of Quantum Technologies, German Aerospace Center (DLR), Söflinger Straße 100, D-89077 Ulm, Germany*

³*Institut für Quantenoptik, Leibniz Universität Hannover, Welfengarten 1, D-30167 Hannover, Germany*

⁴*Hagler Institute for Advanced Study and Department of Physics and Astronomy, Institute for Quantum Science and Engineering (IQSE), Texas A&M AgriLife Research, Texas A&M University, College Station, TX 77843-4242, USA*

Light-pulse atom interferometers constitute powerful quantum sensors for inertial forces. They are based on delocalised spatial superpositions and the combination with internal transitions directly links them to atomic clocks. Since classical tests of the gravitational redshift are based on a comparison of two clocks localised at different positions under gravity, it is promising to explore whether the aforementioned interferometers constitute a competitive alternative for tests of general relativity. Here we present a specific geometry which together with state transitions leads to a scheme that is concurrently sensitive to both violations of the universality of free fall and gravitational redshift, two premises of general relativity. The proposed interferometer does not rely on a superposition of internal states, but merely on transitions between them, and therefore generalises the concept of physical atomic clocks and quantum-clock interferometry. An experimental realisation seems feasible with already demonstrated techniques in state-of-the-art facilities.

INTRODUCTION

The phenomenal advance in accuracy of atomic light-pulse interferometers over the last decades has not only led to high-precision applications in gravimetry [1, 2] and gradiometry [3, 4], but has also opened the possibility to probe fundamental physics such as through measurements of the fine-structure constant to constrain Standard-Model extensions [5, 6], gravitational wave detection [7] or tests of the universality of free fall [8–11]. Since the universality of free fall (UFF) and the universality of gravitational redshift (UGR) form the foundations of general relativity, their violation would directly hint towards new unknown physics. While the former has been tested with light-pulse atom interferometers for two different atomic species to the 10^{-8} level [11], the question whether they can also test UGR has so far not been conclusively answered. In this article we propose the interferometer scheme depicted in Fig. 1, which is sensitive to both violations of UFF and UGR. Whereas a redshift sensitivity may arise from the initialisation of a quantum clock during the interferometer sequence [12], we show that a superposition of internal states is not necessary. Instead, the sensitivity originates solely from the interferometer geometry and the change of internal states.

In general relativity an ideal clock moving along a worldline x^μ measures proper time

$$\tau = \frac{1}{c} \int \sqrt{dx_\mu dx^\mu} \quad (1)$$

where c is the speed of light. This quantity has been connected to the phase of a sufficiently localised matter

wave via the relation [12, 13]

$$\phi = -\omega\tau + S_{\text{em}}/\hbar \quad (2)$$

where $\omega = mc^2/\hbar$ denotes the Compton frequency, m the mass of the atom and S_{em} accounts for the interaction with electromagnetic fields to guide the matter wave. Because of this dependence of the phase on proper time, it is conceivable that atom interferometers provide a platform for tests of special and general relativity.

In a light-pulse interferometer a series of short light pulses drives the atoms into a coherent spatially delocalised superposition and subsequently directs them along the two branches of the interferometer. Upon recombination, the relative phase, which now depends on the proper-time difference $\Delta\tau$ between the two branches, is inferred from the interference pattern.

Since $\Delta\tau$ enters the phase proportional to the Compton frequency ω , it was suggested [14] that, due to its immense value, light-pulse interferometers could be utilised to push the current bounds on violation parameters of UGR by several orders of magnitude. However, standard light-pulse interferometers without internal transitions are insensitive to the gravitational redshift in a uniform gravitational field [12, 15–18] since the proper-time difference between the two branches is independent of gravity in addition to the lack of the concept of a clock. To introduce the latter, one can now envision an experiment where the atoms, which enter the interferometer in an internal superposition, can be viewed as an atomic clock delocalised along the two branches [19]. As a manifestation of Einstein's relation $E = mc^2$, a two-level atom of energy spacing $\hbar\Omega$ with mass m_- in the ground state has a different mass $m_+ = m_- + \hbar\Omega/c^2$ when in the excited state [20–22]. Thus, the Compton frequency be-

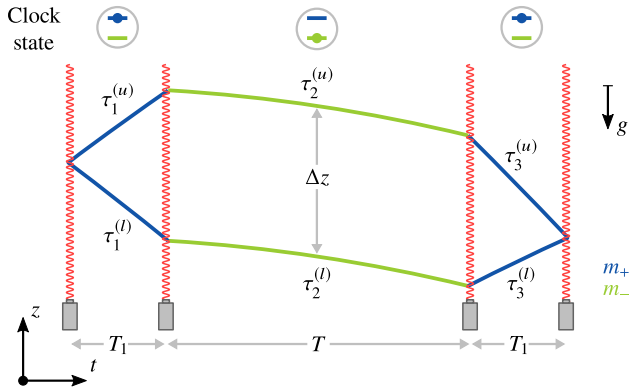


FIG. 1. **Redshift-sensitive geometry.** The interferometer is based on a diffraction scheme where each laser pulse, apart from transferring momentum, also changes the internal state. Initially the input wave packet is split in two components by a $\pi/2$ pulse, which subsequently move in opposite directions with momentum $\pm\hbar k$, where k is the effective wave number of the laser fields. At the second and third laser pulse the wave packets are redirected and finally recombined at the fourth laser pulse by further $\pi/2$ pulses. If initially in the ground state m_- (■), the atoms reside in the excited state m_+ (●) during the first and third segment but occupy the ground state during the middle segment of the interferometer scheme. Note that the atoms are always in the same internal state at equal times (in the laboratory frame).

comes state dependent, that is $\omega_{\pm} = m_{\pm}c^2/\hbar$.

In such quantum-clock interferometers the proper-time difference associated with the interferometer branches leads to a beating in the interference signal [20]. Contrary to symmetric schemes like a Mach-Zehnder geometry or the sequence proposed in the present article, the proper-time difference of an asymmetric Ramsey-Bordé interferometer is non-vanishing, however, of purely special relativistic origin. This geometry allows the implementation of a quantum twin paradox [18], but no coupling between Ω and the linear gravitational acceleration g appears in the phase.

In contrast, if the internal superposition is created within instead of before the interferometer sequence, which corresponds to an initialisation of the clock at a certain variable time, the phase shift becomes sensitive to the gravitational redshift [12].

In the following, we show that a superposition of internal states is not necessary. The redshift sensitivity of our scheme originates from the following property: At each laser pulse the momentum of the atoms and their internal state is changed symmetrically on both branches so that the atoms occupy the same internal state at equal times (in the laboratory frame), see Fig. 1. The experimental implementation of such a configuration will be discussed in the final section.

RESULTS

Relativistic description

To prove the redshift sensitivity, we calculate the phase of such an interferometer scheme to first order in $\Delta m = m_+ - m_-$ and $1/c^2$. The proper time experienced by a particle traveling along a trajectory z with a velocity \dot{z} in a uniform Newtonian gravitational potential gz reads

$$\tau = \int d\tau = \int dt [1 - \dot{z}^2/2c^2 + gz/c^2]. \quad (3)$$

To describe the interaction with the lasers, one has to take the full multi-level structure of the Hamiltonian into account including all the internal-state contributions to the diffraction process. However, after adiabatic elimination and assuming infinitely short laser pulses, the interferometer sequence can be reduced to a branch-dependent description for which the Hamiltonian corresponding to the upper branch ($\alpha = u$) and lower branch ($\alpha = l$)

$$\hat{H}^{(\alpha)} = m_{\pm}c^2 + \frac{\hat{p}^2}{2m_{\pm}} + m_{\pm}g\hat{z} + \hat{V}_{\text{em}}^{(\alpha)}(t, \hat{z}) \quad (4)$$

contains only relativistic contributions in form of different masses m_{\pm} [20–22]. The laser pulses change the internal state and consequently the mass, turning it into a dynamical quantity. The validity of Eq. (4) relies on a differential scheme using inverted internal states, that is $m_+ \leftrightarrow m_-$, either by subsequent measurements or by sending both states concurrently through the interferometer. Consequently, $1/c^2$ corrections to the Hamiltonian either drop out in the differential phase if mass independent, or enter proportional to $\Delta m/c^2$, which is beyond the order considered here. This results in a strong immunity against various relativistic effects such as corrections to the centre-of-mass motion, finite-speed effects of the light as well as higher-order Doppler shifts in the momentum recoil.

The laser-atom interaction is modelled by the potential [16] $\hat{V}_{\text{em}}^{(\alpha)} = -\hbar \sum_{\ell} [k_{\ell}^{(\alpha)} \hat{z} + \varphi_{\ell}^{(\alpha)}] \delta(t - t_{\ell})$, which transfers the momentum $\hbar k_{\ell}^{(\alpha)}$ to branch (α) at $t = t_{\ell}$ and imprints the laser phase $\varphi_{\ell}^{(\alpha)}$ evaluated at the time of the pulse onto the branch. Since in our geometry the atoms are always in the same internal state at equal times (in the laboratory frame) so that m_{\pm} is branch independent, we restrict the discussion to such interferometer schemes. However, the treatment can be generalised if necessary for other schemes.

Defining the proper-time differences $\Delta\tau_n = \tau_n^{(u)} - \tau_n^{(l)}$ for each segment associated with one internal state, we find the phase (see Materials and Methods)

$$\Delta\phi = \Delta\phi_m - \frac{\Omega}{2} \sum_n \lambda_{\pm} \Delta\tau_n \quad (5)$$

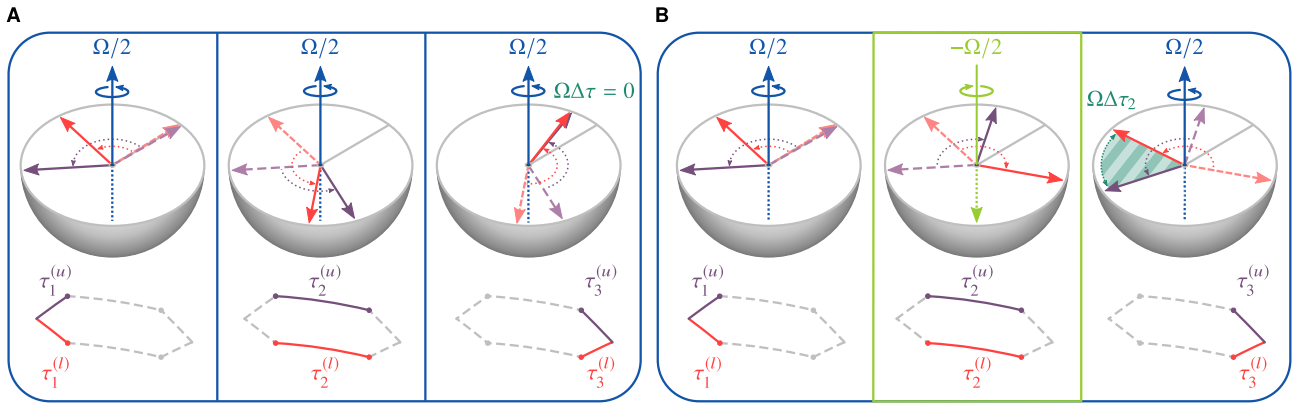


FIG. 2. **Origin of the clock phase.** We compare the clock phases accumulated between the upper branch (violet arrow) and lower branch (red arrow) along the three segments of the interferometer, highlighted in the pictograms below. The accumulation of phases of each branch is depicted by a rotation on the equatorial plane, where the Compton frequency mc^2/\hbar is chosen as a reference. Hence, atoms in the excited state rotate counterclockwise with $\Omega/2$ around the axial vector (■), whereas the axial vector flips when the atoms are in the ground state (■) so that they rotate clockwise with $-\Omega/2$. **A**, If the internal state is not changed during the central segment, the sum of all proper-time differences vanishes so that the clock phase $\Omega\Delta\tau = 0$. **B**, If the internal state is flipped during the central segment, the phase difference does not vanish although $\Delta\tau = 0$. Instead, the phases accumulated during each segment add, and one finds the clock phase $\Omega\Delta\tau_2$, represented by the shaded area. Because the atoms fall during the central segment in parallel at different heights, the phase is proportional to the gravitational redshift.

where $\lambda_{\pm} = \pm 1$ indicates the internal state. Eq. (5) underlines that, to first order in Δm and $1/c^2$, the total phase is the sum of two contributions: (i.) The reference phase $\Delta\phi_m$ is independent of Δm and is obtained with the reference Hamiltonian \hat{H}_m given by Hamiltonian (4) evaluated at the reference mass $m_{\pm} = m$ where $m = (m_+ + m_-)/2$ and we assumed that the interferometer with respect to \hat{H}_m is closed. (ii.) A clock phase as a linear combination of the proper-time differences of each segment calculated for the trajectories generated by \hat{H}_m (not the total Hamiltonian \hat{H}). Since the proper-time difference for each interferometer segment enters proportional to Ω , the differential phase can be associated with the ticking rate of a real (in the case of a superposition of internal states on each branch) or a virtual (in the case of subsequent measurements or mixed states) quantum clock moving simultaneously along the two branches of the interferometer. This clock measures proper-time combinations of the reference trajectories defined by $m_{\pm} = m$.

Redshift-sensitive geometry

For the interferometer scheme proposed in this article we obtain with the help of Eq. (5) the phase $\Delta\phi = \Delta\phi_m - \Omega[\Delta\tau_1 - \Delta\tau_2 + \Delta\tau_3]/2$, where we used λ_{\pm} according to the masses shown in Fig. 1. Like in a Mach-Zehnder interferometer, the symmetry of our scheme leads to a vanishing proper-time difference between the branches (generated by \hat{H}_m) so that $\Delta\tau = \Delta\tau_1 + \Delta\tau_2 + \Delta\tau_3 = 0$. This constraint eliminates the dependence on $\Delta\tau_1$ and

$\Delta\tau_3$ and we obtain

$$\Delta\phi = \Delta\phi_m + \Omega\Delta\tau_2. \quad (6)$$

This result is visualised and explained in more detail in Fig. 2. Since during the central segment the velocities of the atoms on both branches are the same, special-relativistic contributions to proper time cancel and the result calculated with the help of Eq. (3) depends only on the gravitational time-dilation factor

$$\Delta\tau_2 = \frac{g\Delta z}{c^2}T = g\frac{2\hbar kT_1T}{mc^2} \quad (7)$$

which contains the wave number k since the splitting in height $\Delta z = 2\hbar kT_1/m$ is caused by the separation of the branches after the first laser pulse.

The clock phase $\Omega\Delta\tau_2$ in Eq. (6) exactly matches the one measured by two stationary clocks separated by a distance Δz in a uniform gravitational field. Using for example a general formula [18] to obtain the reference phase, we furthermore find $\Delta\phi_m = -2kgT_1(T + T_1)$. Note that this phase can be used for tests of UFF, however, not for UGR, as will be discussed later.

Calculating the exact classical trajectories with respect to Hamiltonian (4) shows that the interferometer is closed to all orders of Δm , giving rise to perfect contrast.

Freely-falling frame

To understand the origin of the phases, we analyse the interferometer in the freely-falling frame. From the perspective of a freely-falling observer the trajectories are straight lines. Because of the relativity of simultaneity

the laser pulses, which in our model act on both branches simultaneously at time t in the laboratory frame, address each branch at slightly different times t' in the freely-falling frame [12]. The different times t and t' are connected by the Rindler transformation

$$t' = t \left[1 + g^2 t^2 / (6c^2) + g z(t) / c^2 \right], \quad (8)$$

which depends on the position of the atoms in the laboratory frame. Consequently, the proper-time difference between the two branches of the central segment is still given by $\Delta\tau_2 = g\Delta z T / c^2$ in the freely-falling frame.

However, within the framework of Hamiltonian (4), it is sufficient to perform a Galilei transformation, that is $z' = z + 1/2gt^2$ since higher corrections are suppressed by at least the factor $\Delta m/c$ in differential measurements. As explained in the caption of Fig. 3, where we plot the transformed trajectories against the laboratory time, it is the deviation of the trajectories due to the change of mass in the presence of the laser pulses which introduces the coupling between Ω and g . In the Materials and Methods we calculate the phase in the freely falling frame with the result

$$\Delta\phi' = \Delta\phi'_m - \frac{\Omega}{2} \sum_n \lambda_{\pm} \Delta\tau'_n, \quad (9)$$

where the proper times in the difference $\Delta\tau'_n = \tau_n^{(u)} - \tau_n^{(l)}$ between the two branches for segment n are defined through the integral

$$\tau' = \int dt \frac{dt'}{dt} \left[1 - \frac{z'^2}{2c^2} \right] \quad (10)$$

to first order in $1/c^2$ and the Rindler time t' was defined in Eq. (8). In the freely-falling frame the reference phase $\Delta\phi'_m$ originates from the Doppler-shifted laser phase $\varphi'_\ell^{(\alpha)} = \varphi_\ell^{(\alpha)} - 1/2gt^2$, which is imprinted on the wave packet at each laser pulse so that $\Delta\phi_m$ takes the same value in both frames. The invariance of the clock phase simply follows from the invariance of the proper time under coordinate transformations and we find $\Delta\phi = \Delta\phi'$. Hence, the clock phase indeed can be interpreted as the sum of proper times along the interferometer branches and it does not arise from the Doppler shift of the frequency or wave vector of the laser.

Violation model

To see whether our interferometer scheme is sensitive to violations of UGR [12], we rely on a consistent parametrisation of a violation model e.g. a dilaton field coupled to the Standard Model and general relativity [23, 24]. In the low-energy and non-relativistic limit the replacement [15] $g \rightarrow (1 + \beta_{\pm})g$ characterises the impact of this massless scalar particle on the phase in Eq. (6). Hence, the coupling of the test mass to gravity is no longer universal but occurs in a state-dependent manner represented by the

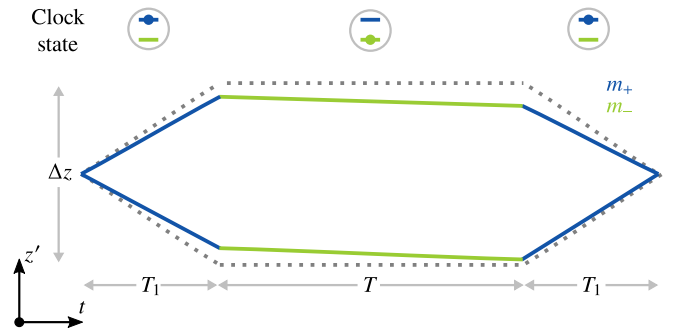


FIG. 3. Origin of the phase in the freely-falling frame. Because of the different masses involved, the classical trajectories (solid lines) deviate from those corresponding to $m_{\pm} = m$ (dashed lines). In particular, at time T_1 where the laser pulses change the mass from m_+ (■) to m_- (■), momentum conservation in the laboratory frame implies $p_f = p_i - \hbar k$ where p_i (p_f) is the momentum before (after) the laser pulse. Performing the Galilei transformation, we find $p'_f - m_- g T_1 = p'_i - m_+ g T_1 - \hbar k$. Consequently, we observe the additional recoil $\Delta p' = -\Delta m g T_1$ in the freely-falling frame resulting in a small gravity-dependent velocity, which results in slightly inclined solid lines in the middle segment. It is this residual recoil which introduces the coupling between Ω and g in the freely-falling frame.

parameter β_{\pm} associated with the mass m_{\pm} , and exactly this non-universal coupling mirrors possible violations of both UFF and UGR. Consequently, the interferometer phase $\Delta\phi$ from Eq. (6) has to be altered into

$$\Delta\phi = \Omega\Delta\tau_2 (1 + \alpha) - 2kgT_1 (T + T_1) (1 + \beta_+) \quad (11)$$

to include a factor $\Delta m \alpha = m (\beta_+ - \beta_-)$. Note that we neglected terms of the form $\Delta m \beta_{\pm}$.

When comparing the interference signals of two stationary and independent clocks, we find a similar dependence on α . Consequently, the interferometer scheme proposed in this article can be used to set bounds on violation parameters for the gravitational redshift. Contrary to this UGR parametrisation, possible UFF violations are represented by the difference $\beta_+ - \beta_-$ only.

As mentioned above, the validity of the presented scheme is premised on a differential measurement with inverted internal states. This measurement procedure causes the differential phase

$$\delta\phi = 2\Omega\Delta\tau_2 (1 + \alpha) - 2kgT_1 (T + T_1) (\beta_+ - \beta_-), \quad (12)$$

which offers the possibility to test *both* UGR (first term through α) as well as UFF (second term through $\beta_+ - \beta_-$). These two fundamental tests can be differentiated by varying the duration T of the central segment so that our scheme provides access to two aspects of the foundations of general relativity, in contrast to stationary clocks or conventional atom interferometers. However, contrary to UFF tests with different atomic species [9],

the proposed scheme compares two internal states of the same atom for which violation parameters were recently bounded to the 10^{-10} level [25].

DISCUSSION

An experimental realisation requires atomic species with large internal transition frequencies. Recent experiments have demonstrated the coherent control of ^{88}Sr [26] with a transition frequency of the order of a few hundred THz in the optical regime.

The implementation of our scheme requires a diffraction mechanism combining a momentum transfer with a change of the internal states symmetrically on both branches. This is naturally the case for double-Raman scattering [27], see Fig. 4A, which has also been successfully implemented in a gravimeter [28]. However, an analogue scheme for optical Raman transitions requires laser frequencies in the ultraviolet and has not been implemented to date. In addition to these challenging experimental aspects, the lasers address each branch at slightly different times because of the finite speed of light. However, for the same momentum transfer $\hbar k$ in the state-inversed scheme, the leading-order effect caused by this non-simultaneity cancels in the differential phase, while the remaining contributions are suppressed by a factor $1/c$ compared to the phase of interest. The value of k can be fixed for both experimental runs by chirping the lasers appropriately, which, however, requires four laser frequencies to realise the double-Raman scheme. As a promising alternative to double-Raman diffraction, recent results [29] can be generalised so that each pulse is decomposed into a momentum-transfer pulse based on double-Bragg diffraction [30] or a dual-lattice Bloch beam splitter [31] and a state-changing pulse employing the Doppler-free optical E1-M1 two-photon transition [32] accessible for example in ^{88}Sr or ^{170}Yb atoms, see Fig. 4B. The latter consists of two counter-propagating beams with equal frequencies in the laboratory frame that correspond to half the frequency of the clock transition and guarantee that the transition takes place simultaneously on both interferometer arms with respect to the laboratory frame [12]. Since the momentum transfer must not change upon state inversion, one possibility is to perform double-Bragg diffraction or lattice beam splitters at the magic wavelength [33] on the respective states of the clock transition. Moreover, in both cases one can further increase the separation of the two interferometer branches using large-momentum transfer techniques such as Bloch oscillations [6, 31, 34]. Specifically, assuming an effective $k = 508\bar{k}$ with $\bar{k} \approx 10^6\text{m}^{-1}$ and interferometer times of a few hundred milliseconds, which are achievable in a 10 m atomic fountain tower, the phase of interest becomes of the order of milliradians. Assuming a resolution close to shot noise and

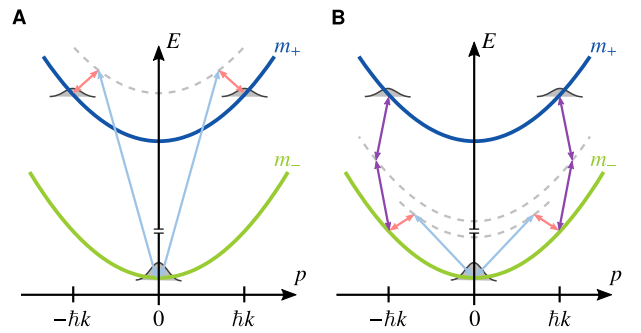


FIG. 4. **Energy-momentum diagrams of state- and momentum-changing diffraction schemes.** **A**, Double-Raman diffraction is based on two two-photon processes mediated by a virtual state (dashed line) and generated by two counter-propagating optical lattices (symbolised by the red and blue arrows). Initially in the ground state, denoted by its mass m_- (■), it is elevated to the excited state with m_+ (■) and simultaneously diffracted into a superposition of two opposite momenta $\pm\hbar k$. The parabolas highlight the dispersion relation in each state and the condition for a resonant transition. **B**, A sequence of double-Bragg diffraction (red and blue arrows) that first diffracts within the ground state from two counter-propagating lattices into two opposing momentum states in combination with a Doppler-free E1-M1 two-photon transitions (purple arrows) reproduces the double-Raman scheme. However, the recoil-less transitions can be performed with optical frequencies so that a different range of clock frequencies can be addressed compared to conventional double-Raman diffraction.

atom numbers of 10^6 , this phase should be resolvable within a few hundred shots.

We stress again that the validity of the scheme is based on inversion of the internal states in subsequent measurements so that phase contributions independent of Δm cancel out in the differential phase. As a consequence, also corrections to the centre-of-mass Hamiltonian are additionally suppressed by the factor $1/c^2$ compared to the phase of interest.

It should be noted that the deleterious effects discussed above also slightly open the interferometer. However, the resulting uncontrollable dependence on the initial conditions of the wave packet which might differ from shot to shot is extremely small and can be neglected. The more dramatic dependence on the initial conditions originating from the influence of gravity gradients and rotations are assumed to be successfully mitigated [35–37].

Finally, the approximation of infinitely short laser pulses is justified for pulse times Δt much smaller than the total interferometer time T [38]. Due to the differential measurement, finite-pulse-time effects are suppressed by the factor $\Delta t/T \ll 1$ compared to the phase of interest.

Since the phase difference of two atomic clocks separated by Δz takes the form $\Omega T(1 + \alpha)g\Delta z/c^2$ that also

arises in our geometry, classical tests of UGR display in principle the same sensitivity for the same parameters Ω , T and Δz , neglecting technical noise for the moment. Therefore, atom interferometers are intrinsically limited by the dimensions of the apparatus, namely T and Δz , whereas there is in principle no bound on the separation of two independent clocks. However, the conceptual relevance of atom interferometric tests of UGR relies on the use of single, delocalised quantum objects instead of two independent clocks as used in conventional tests. Hence, our geometry allows probing the light-matter coupling and relativistic effects with a delocalised particle, whereas clocks can probe the laser field only at localised and independent points in spacetime. Additionally, light-pulse-based interferometers with atoms in free fall offer a complementary approach to atomic clocks since effects such as limited coherence times inside atomic traps due to continuous electromagnetic interactions have not to be actively mitigated [39].

MATERIALS AND METHODS

Phase in the laboratory frame

The phase $\Delta\phi$ and contrast C of an interferometer are defined by the expectation value

$$\langle \hat{U}^{(l)\dagger} \hat{U}^{(u)} \rangle = C e^{i\Delta\phi}, \quad (13)$$

where $\hat{U}^{(l)}$ and $\hat{U}^{(u)}$ are the time-evolution operators with respect to Hamiltonian (4) corresponding to the upper branch ($\alpha = u$) and the lower branch ($\alpha = l$). To calculate the phase to first order in $\Delta m = m_+ - m_-$, we Taylor-expand Eq. (4) around $m_{\pm} = m + \lambda_{\pm} \Delta m / 2$ where $m = (m_- + m_+) / 2$ is the reference mass and the dynamical variable λ_{\pm} with $\lambda_- = -1$ and $\lambda_+ = +1$ indicates the internal state. This approximation allows for the decomposition $\hat{H}^{(\alpha)} = \hat{H}_m^{(\alpha)} + \hat{H}_{\Delta m}^{(\alpha)}$ with

$$\hat{H}_{\Delta m}^{(\alpha)} = \lambda_{\pm} \frac{\Delta m c^2}{2} [1 - (\hat{p}/m)^2 / 2c^2 + g\hat{z}/c^2] \quad (14)$$

and $\hat{H}_m^{(\alpha)}$ is Eq. (4) evaluated at $m_{\pm} = m$. We now assume that for the reference Hamiltonian $\hat{H}_m^{(\alpha)}$, as in the case of our scheme, the interferometer is closed leading to a perfect wave-packet overlap at the end of the interferometer sequence. Defining $\hat{U}_m^{(\alpha)}$ as the time-evolution operator with respect to $\hat{H}_m^{(\alpha)}$, this fact translates into $\hat{U}_m^{(l)\dagger} \hat{U}_m^{(u)} = e^{i\Delta\phi_m}$, where $\Delta\phi_m$ is merely a c -number. When we transform Eq. (13) into the interaction picture with respect to $\hat{H}_m^{(\alpha)}$, we find

$$\hat{U}^{(l)\dagger} \hat{U}^{(u)} = \hat{U}_{\Delta m, I}^{(l)\dagger} \hat{U}_m^{(l)\dagger} \hat{U}_m^{(u)} \hat{U}_{\Delta m, I}^{(u)} = e^{i\Delta\phi_m} \hat{U}_{\Delta m, I}^{(l)\dagger} \hat{U}_{\Delta m, I}^{(u)}. \quad (15)$$

Here, $\hat{U}_{\Delta m, I}^{(\alpha)}$ is the time-evolution operator associated with $\hat{H}_{\Delta m, I}^{(\alpha)}$ where the subscript I denotes the interaction picture with respect to $\hat{H}_m^{(\alpha)}$. The transformation

into the interaction picture amounts to replacing the momentum and position operators in Eq. (14) by their respective solution of the Heisenberg equation of motion generated by $\hat{H}_m^{(\alpha)}$. They take the form $\hat{p}(t) = \hat{p} + p(t)$ and $\hat{z}(t) = \hat{z} + \hat{p}t/m + z(t)$, where $p(t)$ and $z(t)$ (without hat) denote the classical trajectories. To combine the two time-evolution operators on the right-hand side of Eq. (15), we disregard the time-ordering consistently to first order in Δm as evident from the Magnus expansion [40]. To the same order we furthermore merge the two exponents. Since all wave-packet effects are common to both branches, they cancel and the interferometer is closed.

Defining the proper-time differences $\Delta\tau_n = \tau_n^{(u)} - \tau_n^{(l)}$ for each segment associated with one internal state, we find the phase

$$\Delta\phi = \Delta\phi_m - \frac{\Omega}{2} \sum_n \lambda_{\pm} \Delta\tau_n \quad (16)$$

with the help of $\dot{z}(t) = p(t)/m$ and Eq. (3) and after introducing the transition frequency $\Omega = \Delta m c^2 / \hbar$.

Phase in the freely-falling frame

To transform the Hamiltonian (4) into the freely-falling frame, for example by returning to the classical Lagrangian picture, we perform the Galilei transformation and partial integration to obtain the quantised Hamiltonian

$$\hat{H}'^{(\alpha)} = m_{\pm} c^2 + \frac{\hat{p}'^2}{2m_{\pm}} + \hat{V}_{\text{em}}'^{(\alpha)} - m_{\pm} g^2 t^2 - \dot{m}_{\pm} \hat{z}' g t. \quad (17)$$

Here, \dot{m}_{\pm} is the time derivative of the mass which is only non-vanishing during the laser pulses. The transformed laser-atom interaction takes the form $\hat{V}_{\text{em}}'^{(\alpha)} = -\hbar \sum_{\ell} [k_{\ell}^{(\alpha)} \hat{z}' + \varphi_{\ell}'^{(\alpha)}] \delta(t - t_{\ell})$, where $\varphi_{\ell}'^{(\alpha)} = \varphi_{\ell}^{(\alpha)} - 1/2 g t^2$ is imprinted on the wave packet at each laser pulse. We again decompose the Hamiltonian through a Taylor expansion into $\hat{H}'^{(\alpha)} = \hat{H}_m'^{(\alpha)} + \hat{H}_{\Delta m}'^{(\alpha)}$ with $\hat{H}_m'^{(\alpha)} = \hat{p}'^2 / 2m + \hat{V}_{\text{em}}'^{(\alpha)}$ and a Hamiltonian taking into account the changes of the mass

$$\hat{H}_{\Delta m}'^{(\alpha)} = \lambda_{\pm} \frac{\Delta m c^2}{2} \left[1 - \frac{(\hat{p}'/m)^2}{2c^2} - \frac{g^2 t^2}{c^2} \right] - \dot{m}_{\pm} \hat{z}' g t \quad (18)$$

to first order in Δm , where we discarded global phases. By following the derivation of Eq. (5), we find, after recalling $\dot{z}'(t) = p'(t)/m$ and partial integration of the last term in Eq. (18) the phase

$$\Delta\phi' = \Delta\phi'_m - \frac{\Omega}{2} \sum_n \lambda_{\pm} \Delta\tau'_n \quad (19)$$

in the freely falling frame. To first order in $1/c^2$ the proper-time difference $\Delta\tau'_n = \tau_n'^{(u)} - \tau_n'^{(l)}$ between the

two branches for segment n is defined via the integral

$$\tau' = \int dt \frac{dt'}{dt} \left[1 - \frac{\dot{z}'^2}{2c^2} \right] \quad (20)$$

where the Rindler time, which was defined in Eq. (8), was identified.

ACKNOWLEDGEMENTS

E.G., A.F., F.D.P. and C.U. thank Holger Müller for fruitful discussions at the Quantum Metrology and Physics beyond the Standard Model conference in Hannover. Furthermore, we thank Sina Loriani and Thomas Hensel for extensive discussions and feedback regarding the presented material.

This work is supported by the German Aerospace Center (DLR) with funds provided by the Federal Ministry for Economic Affairs and Energy (BMW) due to an enactment of the German Bundestag under Grant Nos. DLR 50WM1556 and 50WM1956. C. S., D. S. and E. M. R. thank CRC 1227 (DQ-mat) project B07, the EXC 2123 “Quantum Frontiers” within the research units B02 and B05, the QUEST-LFS and “Niedersächsisches Vorab” through “Förderung von Wissenschaft und Technik in Forschung und Lehre” for the initial funding of research in the new DLR-SI Institute. C. S. thanks “Niedersächsisches Vorab” through the “Quantum- and Nano-Metrology (QUANOMET)” initiative within the project QT3. D. S. gratefully acknowledges funding by the Federal Ministry of Education and Research (BMBF) through the funding program Photonics Research Germany under contract number 13N14875. C. U., F. D. P., A. F., A. R., E. G., and W. P. S. thank the Ministry of Science, Research and Arts Baden-Württemberg for financially supporting the work of IQST. Moreover, W. P. S. is grateful to Texas A&M University for a Faculty Fellowship at the Hagler Institute for Advanced Study as well as to Texas A&M AgriLife for its support.

-
- [1] A. Peters, K. Y. Chung, and S. Chu, “Measurement of gravitational acceleration by dropping atoms,” *Nature* **400**, 849–852 (1999).
- [2] T. Farah, C. Guerlin, A. Landragin, P. Bouyer, S. Gaffet, F. Pereira Dos Santos, and S. Merlet, “Underground operation at best sensitivity of the mobile LNE-SYRTE cold atom gravimeter,” *Gyroscopy Navig.* **5**, 266–274 (2014).
- [3] M. Snadden, J. McGuirk, P. Bouyer, K. Haritos, and M. Kasevich, “Measurement of the Earth’s gravity gradient with an atom interferometer-based gradiometer,” *Phys. Rev. Lett.* **81**, 971–974 (1998).
- [4] P. Asenbaum, C. Overstreet, T. Kovachy, D. D. Brown, J. M. Hogan, and M. A. Kasevich, “Phase shift in an atom interferometer due to spacetime curvature across its wave function,” *Phys. Rev. Lett.* **118**, 183602 (2017).
- [5] A. Wicht, J. M. Hensley, E. Sarajlic, and S. Chu, “A preliminary measurement of the fine structure constant based on atom interferometry,” *Phys. Scr.* **T102**, 82–88 (2002).
- [6] R. H. Parker, C. Yu, W. Zhong, B. Estey, and H. Müller, “Measurement of the fine-structure constant as a test of the Standard Model,” *Science* **360**, 191–195 (2018).
- [7] P. W. Graham, J. M. Hogan, M. A. Kasevich, and S. Rajendran, “Resonant mode for gravitational wave detectors based on atom interferometry,” *Phys. Rev. D* **94**, 104022 (2016).
- [8] S. Fray, C. A. Diez, T. W. Hänsch, and M. Weitz, “Atomic interferometer with amplitude gratings of light and its applications to atom based tests of the equivalence principle,” *Phys. Rev. Lett.* **93**, 240404 (2004).
- [9] D. Schlippert, J. Hartwig, H. Albers, L. L. Richardson, C. Schubert, A. Roura, W. P. Schleich, W. Ertmer, and E. M. Rasel, “Quantum test of the universality of free fall,” *Phys. Rev. Lett.* **112**, 203002 (2014).
- [10] M. G. Tarallo, T. Mazzoni, N. Poli, D. V. Sutyryn, X. Zhang, and G. M. Tino, “Test of Einstein equivalence principle for 0–spin and half-integer-spin atoms: Search for spin-gravity coupling effects,” *Phys. Rev. Lett.* **113**, 023005 (2014).
- [11] L. Zhou, S. Long, B. Tang, X. Chen, F. Gao, W. Peng, W. Duan, J. Zhong, Z. Xiong, J. Wang, Y. Zhang, and M. Zhan, “Test of equivalence principle at 10^{-8} level by a dual-species double-diffraction Raman atom interferometer,” *Phys. Rev. Lett.* **115**, 013004 (2015).
- [12] A. Roura, “Gravitational redshift in quantum-clock interferometry,” [arXiv:1810.06744](https://arxiv.org/abs/1810.06744) (2018).
- [13] S. Dimopoulos, P. W. Graham, J. M. Hogan, and M. A. Kasevich, “General relativistic effects in atom interferometry,” *Phys. Rev. D* **78**, 042003 (2008).
- [14] H. Müller, A. Peters, and S. Chu, “A precision measurement of the gravitational redshift by the interference of matter waves,” *Nature* **463**, 926–930 (2010).
- [15] P. Wolf, L. Blanchet, C. J. Bordé, S. Reynaud, C. Salomon, and C. Cohen-Tannoudji, “Does an atom interferometer test the gravitational redshift at the Compton frequency?” *Class. Quantum Grav.* **28**, 145017 (2011).
- [16] W. P. Schleich, D. M. Greenberger, and E. M. Rasel, “A representation-free description of the Kasevich-Chu interferometer: A resolution of the redshift controversy,” *New J. Phys.* **15**, 013007 (2013).
- [17] E. Giese, A. Friedrich, F. Di Pumpo, A. Roura, W. P. Schleich, D. M. Greenberger, and E. M. Rasel, “Proper time in atom interferometers: Diffractive versus specular mirrors,” *Phys. Rev. A* **99**, 013627 (2019).
- [18] S. Loriani, A. Friedrich, C. Ufrecht, F. Di Pumpo, S. Kleinert, S. Abend, N. Gaaloul, C. Meiners, C. Schubert, D. Tell, É. Wodey, M. Zych, W. Ertmer, A. Roura, D. Schlippert, W. P. Schleich, E. M. Rasel, and E. Giese, “Interference of clocks: A quantum twin paradox,” *Sci. Adv.* **5**, eaax8966 (2019).
- [19] S. Sinha and J. Samuel, “Atom interferometry and the gravitational redshift,” *Class. Quantum Grav.* **28**, 145018 (2011).
- [20] M. Zych, F. Costa, I. Pikovski, and Č. Brukner, “Quantum interferometric visibility as a witness of general relativistic proper time,” *Nat. Commun.* **2**, 505 (2011).
- [21] M. Sonnleitner and S. M. Barnett, “Mass-energy and anomalous friction in quantum optics,” *Phys. Rev. A* **98**, 042106 (2018).

- [22] P. K. Schwartz and D. Giulini, “Post-Newtonian Hamiltonian description of an atom in a weak gravitational field,” *Phys. Rev. A* **100**, 052116 (2019).
- [23] T. Damour and J. F. Donoghue, “Equivalence principle violations and couplings of a light dilaton,” *Phys. Rev. D* **82**, 084033 (2010).
- [24] T. Damour, “Theoretical aspects of the equivalence principle,” *Class. Quantum Grav.* **29**, 184001 (2012).
- [25] K. Zhang, M.-K. Zhou, Y. Cheng, L.-L. Chen, Q. Luo, W.-J. Xu, L.-S. Cao, X.-C. Duan, and Z.-K. Hu, “Testing the universality of free fall at 10^{-10} level by comparing the atoms in different hyperfine states with Bragg diffraction,” [arXiv:1805.07758](https://arxiv.org/abs/1805.07758) (2018).
- [26] L. Hu, N. Poli, L. Salvi, and G. M. Tino, “Atom interferometry with the Sr optical clock transition,” *Phys. Rev. Lett.* **119**, 263601 (2017).
- [27] T. Lévêque, A. Gauguier, F. Michaud, F. Pereira Dos Santos, and A. Landragin, “Enhancing the area of a Raman atom interferometer using a versatile double-diffraction technique,” *Phys. Rev. Lett.* **103**, 080405 (2009).
- [28] N. Malossi, Q. Bodart, S. Merlet, T. Lévêque, A. Landragin, and F. Pereira Dos Santos, “Double diffraction in an atomic gravimeter,” *Phys. Rev. A* **81**, 013617 (2010).
- [29] M. Jaffe, V. Xu, P. Haslinger, H. Müller, and P. Hamilton, “Efficient adiabatic spin-dependent kicks in an atom interferometer,” *Phys. Rev. Lett.* **121**, 040402 (2018).
- [30] H. Ahlers, H. Müntinga, A. Wenzlawski, M. Krutzik, G. Tackmann, S. Abend, N. Gaaloul, E. Giese, A. Roura, R. Kuhl, C. Lämmerzahl, A. Peters, P. Windpassinger, K. Sengstock, W. P. Schleich, W. Ertmer, and E. M. Rasel, “Double Bragg interferometry,” *Phys. Rev. Lett.* **116**, 173601 (2016).
- [31] Z. Pagel, W. Zhong, R. H. Parker, Ch. T. O’und, N. Y. Yao, and H. Müller, “Bloch beamsplitters and dual-lattice methods for atom interferometry,” [arXiv:1907.05994](https://arxiv.org/abs/1907.05994) (2019).
- [32] E. A. Alden, K. R. Moore, and A. E. Leanhardt, “Two-photon $E1$ - $M1$ optical clock,” *Phys. Rev. A* **90**, 012523 (2014).
- [33] Hidetoshi Katori, Masao Takamoto, V. G. Pal’chikov, and V. D. Ovsiannikov, “Ultrastable optical clock with neutral atoms in an engineered light shift trap,” *Phys. Rev. Lett.* **91**, 173005 (2003).
- [34] T. Kovachy, P. Asenbaum, C. Overstreet, C. A. Donnelly, S. M. Dickerson, A. Sugarbaker, J. M. Hogan, and M. A. Kasevich, “Quantum superposition at the half-metre scale,” *Nature* **528**, 530–533 (2015).
- [35] A. Roura, “Circumventing Heisenberg’s uncertainty principle in atom interferometry tests of the equivalence principle,” *Phys. Rev. Lett.* **118**, 160401 (2017).
- [36] C. Overstreet, P. Asenbaum, T. Kovachy, R. Notermans, J. M. Hogan, and M. A. Kasevich, “Effective inertial frame in an atom interferometric test of the equivalence principle,” *Phys. Rev. Lett.* **120**, 183604 (2018).
- [37] S. Lan, P. Kuan, B. Estey, P. Haslinger, and H. Müller, “Influence of the Coriolis force in atom interferometry,” *Phys. Rev. Lett.* **108**, 090402 (2012).
- [38] A. Bertoldi, F. Minardi, and M. Prevedelli, “Phase shift in atom interferometers: Corrections for nonquadratic potentials and finite-duration laser pulses,” *Phys. Rev. A* **99**, 033619 (2019).
- [39] Ross B. Hutson, Akihisa Goban, G. Edward Marti, Lindsay Sonderhouse, Christian Sanner, and Jun Ye, “Engineering quantum states of matter for atomic clocks in shallow optical lattices,” *Phys. Rev. Lett.* **123**, 123401 (2019).
- [40] C. Ufrecht, “Theoretical approach to high-precision atom interferometry,” *Ph.D. thesis, Universität Ulm* (2019).